Large Area MOVPE Growth of Topological Insulator Bi$_2$Te$_3$ Epitaxial Layers on i-Si (111)

Arun Kumar[†], Raimondo Cecchini[‡], Lorenzo Locatelli[†], Claudia Wiemer[†], Christian Martella[†], Lucia Nasi[§], Laura Lazzarini[§], Roberto Mantovan[*†] and Massimo Longo[*∥]

† CNR - Institute for Microelectronics and Microsystems, Via C. Olivetti 2, 20864, Agrate Brianza, Italy

‡ CNR - Institute for Microelectronics and Microsystems, Via Gobetti, 101, 40129, Bologna, Italy

§ CNR - Institute of Materials for Electronics and Magnetism, Parco Area delle Scienze, 7/A, 43124 Parma, Italy

∥ CNR - Institute for Microelectronics and Microsystems, Via del Fosso del Cavaliere, 100, 00133, Rome, Italy

[*]To whom correspondence should be addressed. E-mail: roberto.mantovan@mdm.imm.cnr.it, massimo.longo@artov.imm.cnr.it

Abstract

Bi$_2$Te$_3$ is attracting a renewed interest, due to its topological insulator properties; however, even using advanced physical and chemical deposition techniques, the growth of high-crystal quality layers on substrates allowing its technological employment, such as Si, is very challenging, due to the structural complexity of Bi$_2$Te$_3$. In this work, we present the optimized large area growth of topological insulator Bi$_2$Te$_3$ epitaxial layers on un-buffered i-Si (111) substrates via Metal-Organic Vapor Phase Epitaxy (MOVPE), which is of crucial importance for future integration into CMOS compatible spintronic devices. We found that the key to maximizing the layer quality requires a balanced control of the reactor pressure (P), growth temperature (T), and growth time (t). Within a proper parameter window, the grown Bi$_2$Te$_3$ thin layers are crystalline, stoichiometric, and highly uniform, also at the local scale. They exhibit a rhombohedral crystalline structure, and they are [001] out-of-plane oriented on the i-Si (111) substrate. Low temperature magnetoresistance measurements revealed clear Weak Antilocalization (WAL) effects, demonstrating that the optimized MOVPE - grown Bi$_2$Te$_3$ is a topological insulator, hence opening further possibilities for its technology-transfer to innovative devices.

KEYWORDS: Bi$_2$Te$_3$, MOCVD, MOVPE, epitaxial layers, topological insulators

Introduction

Bismuth telluride (Bi_2Te_3) thin layers are being intensively investigated, mainly due to their exceptional performances as thermoelectric materials and perspective applications as topological insulators (TIs) [1–5]. Bi_2Te_3 is considered to be the best thermoelectric material at ~100 °C [6,7] and it has been confirmed to have TI properties by angle-resolved photoemission spectroscopy [3,8], magneto-transport measurements [9], and scanning tunnelling microscopy analysis [10]. TIs are insulating materials in the bulk, while presenting metallic conducting surface states, which are topologically protected with spin polarization locked to crystal momentum [5]. The unique electronic and optical properties associated with these surface states make them strong candidates to study innovative quantum phenomena and to explore practical applications for quantum computing, spintronics and nano technological devices [11,12]. Since the most interesting properties of the TIs are related to their surface, the first step for exploiting the unique properties of Bi_2Te_3 is to have homogeneous, wafer-scale, large-domain size and defect-free layer growth, with a high surface-to-bulk ratio [8,13,14].

Various deposition techniques, such as sputtering [15,16], evaporation [17,18], pulsed laser deposition [19,20], physical vapor transport [21–23], electrochemical deposition [24], molecular beam epitaxy (MBE) [8,25–30] have been employed to grow continuous Bi_2Te_3 films on different substrates. The high cost of the complex equipment with operation in ultra-high vacuum conditions and the low yield of the MBE process can limit its applications in the industry [14]. Compared to other methods, Metal-Organic Chemical Vapour Deposition (MOCVD) (Metal-Organic Vapour Phase Epitaxy, MOVPE in the case of epitaxial deposition) allows for the preparation of highly crystalline, uniform thin layers, with good control of the composition; by using the optimized conditions, it can be potentially suitable for large-scale industrial production. Indeed, MOCVD has been already employed to grow continuous Bi_2Te_3 layers [1,31–35] but most of the reported studies are limited to substrates like Pyrex [31], SiO_2 [32], Sapphire [33], GaAs [34,35]. However, the quality of this class of layers has not been significantly improved, which could not be compatible with device integration. Most importantly, the direct growth of high quality Bi_2Te_3 layers on silicon substrates would be a great advantage for their application in microelectronic devices.

Motivated by its potential technological impact, in this work we present a method for growing controlled epitaxial Bi_2Te_3 layers on i-Si (111) by MOVPE on large area substrates. To our knowledge, there are no reports in the literature on a successful growth of this type. Beside the role of the [111] orientation of the substrate, we report how the fine-tuning of the precursor's

partial pressure ratio, growth pressure, temperature, and time are necessary to achieve the required crystalline quality. Our work revealed step by step growth of high crystal quality Bi_2Te_3 layers in the typical rhombohedral crystalline structure having c - lattice out-of-plane to the i-Si (111) substrate. To study the electrical conduction properties of the grown layers, the grown Bi_2Te_3 layers were also analyzed by Magnetoresistance (MR) measurements. A clear Weak Antilocalization (WAL) effect was found, thus proving the topological insulating character of the Bi_2Te_3 layers.

Experimental

The employed substrates were i-Si (111) and i- Si (100) oriented wafers. Before deposition, the substrates were treated with HF (5% in deionized H_2O) for 3 min, thoroughly rinsed with deionized H_2O, and N_2-dried. Then, they were rapidly loaded into the MOVPE chamber. The Bi_2Te_3 layers were grown with an AIXTRON AIX 200/4 MOCVD tool, equipped with an IR-heated 4″ rotating graphite susceptor. Electronic grade Trimethylbismuth ($BiMe_3$) and Di-isopropyltellurium (DiPTe) were employed as Bi and Te precursors, respectively. The depositions were carried out in the temperature (T) range of 300 - 400 °C for a duration (t) of 30-240 min, at a pressure (P) of 25-150 mbar pressure, with a total flow of 2000-4500 l min^{-1} and setting the precursors vapor pressures at 4.20 and 7.80 x 10^{-3} mbar for $BiMe_3$ and DiPTe, respectively.

X-ray Diffraction (XRD) patterns were acquired with an HRXRD IS2000 tool, equipped with a Cu Kα radiation source, a four-circle goniometer, and a curved 120° position-sensitive detector (Inel CPS-120).

Atomic Force Microscopy (AFM) images were obtained by a Bruker Dimension Edge instrument in non-contact mode, using a sharp silicon AFM probe (TESPA, Bruker) with a typical radius of curvature in the 8-12 nm range. A polynomial background correction was applied to the raw data. Surface roughness was reported as Root Mean Square roughness (RMS roughness) and expressed in nm.

Raman characterization was performed in a z-backscattering geometry by using a Renishaw In-via Spectrometer, equipped with the 1.96 eV (wavelength 633 nm) line of a continuous He-Ne laser (class 3B). The laser beam was focused onto the sample by a 50× (0.75 numerical aperture) Leica objective. The beam power at the sample was maintained below 1 mW to avoid laser-induced heating on the surface and sample damage.

Scanning Electron Microscopy (SEM) images were acquired with a ZEISS Supra 40 field emission scanning electron microscope, at an acceleration voltage of 15 kV. Cross-section images were collected at a tilting angle of 10°.

Transmission Electron Microscopy (TEM) analyses were performed using a JEOL 2200FS microscope working at 200 kV, equipped with an Energy Dispersive X-ray Spectrometer (EDX), two high-angle annular dark-field (HAADF) detectors, and an in-column energy (Omega) filter. The cross-sectional view samples were prepared using standard mechano-chemical procedures and finished by ion beam thinning.

Magnetoresistance (MR) measurements were carried out at 5.5 K using a four-point probe in the van der Pauw configuration. Magnetic fields up to 0.8 T were applied both perpendicularly and parallelly to the sample's plane (and current). The measurements were conducted at a constant applied current of 100 µA, by measuring the longitudinal voltage changes during the magnetic field scan. In particular, the measurements of the sheet resistance (Rs) as a function of the magnetic field (B) were recorded on (1x1) cm^2 substrates, cleaved from the grown samples without any patterning or capping, to avoid any damage to the layers. The values obtained for the sheet resistances is then reversed, referred to its value at zero field and expressed in unit of e^2/h. The signal obtained from this operation is defined as $\Delta\sigma$ and it was used to visualize and compare directly the analysed data.

Results & Discussions

A systematic preliminary growth study was performed as a function of the main deposition parameters (temperature, pressure and time), after identifying the proper super-saturation conditions leading to material deposition (see Supporting Information Figure S1, S2, S3). The effect of an i-Si (100) oriented substrate was also investigated, as described in the Supporting Information (see Figure S4). The optimized growth conditions of Bi_2Te_3 layers on i-Si (111) were found to be a temperature of 350 °C, a pressure of 75 mbar, and for 180 min growth time. The sample morphology is reported in Figure 1 (a, b), where the plan and cross-sectional SEM micrographs are shown. From the cross-section SEM images, it can be seen that the Bi_2Te_3 layers have a uniform thickness of about 90 nm and continuous, flat surfaces.

The surface morphology of the optimized Bi_2Te_3 thin layers was characterized by AFM. A high-resolution topographic image (500 nm x 500 nm) of the layer and a representative height line profile are reported in Figure 1 (c) and (d), respectively. The topography shows a terrace-step surface morphology uniformly distributed over the whole sample area. Terraces extend up

to the micron range in the lateral dimension (see Supporting Information Figure S5), while the line profile shows step height of the order of 1 nm, compatible with the thickness of a single quintuple layer (QL) of the Bi_2Te_3 crystal structure. Indeed, the binary Bi_2Te_3 compound presents a rhombohedral layered structure with space group $R\bar{3}m$ (SG #166) and lattice parameters a = 0.4395 nm and c = 3.044 nm (ICSD 74348). Its unit cell stacks three building blocks along the [001] direction, separated by van der Waals gaps, and each one rotated by 120° with respect to the one below. Each block (QL), is composed by five atomic planes in the sequence -Te-Bi-Te-Bi-Te-, as reported in Supporting Information Figure S6. There is a strong affinity to complete each QL before a new QL nucleates on the surface, which results in a surface structure that features QL steps [36,37]. Additionally, the RMS roughness extracted from the AFM analysis (~ 0.5 nm) revealed that the optimized growth leads to an flat surface morphology, comparable with those reported for Bi_2Te_3 layers grown by MBE [26,27,38–40].
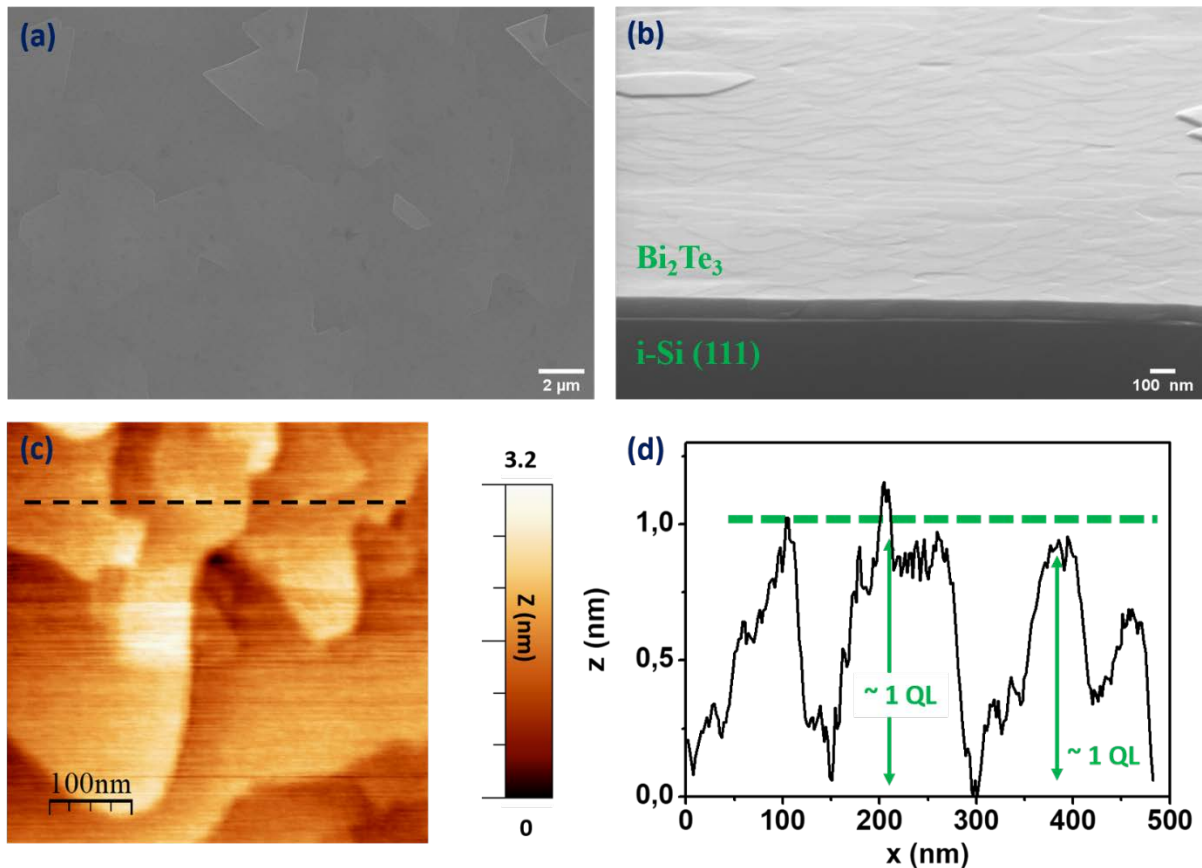

Figure 1. (a) Plan view SEM image, (b) Tilted cross-sectional SEM image, (c) AFM image, and (d) its corresponding height line profile for an optimized Bi_2Te_3 layer, grown on i-Si (111) at T = 350 °C, P = 75 mbar, t = 180 min.

The grown materials were also studied by micro-Raman spectroscopy, as shown in Figure 2(a). The Raman spectrum exhibits two main vibrational peaks located at ~ 102 and ~133 cm^{-1}. This finding is compelling evidence of the high quality of the grown Bi$_2$Te$_3$ since the observed peaks are well-consistent with the previously reported in-plane E^2_g and out-of-plane A$^2_{1g}$ phonon modes of the Bi$_2$Te$_3$ single crystal, respectively [41].
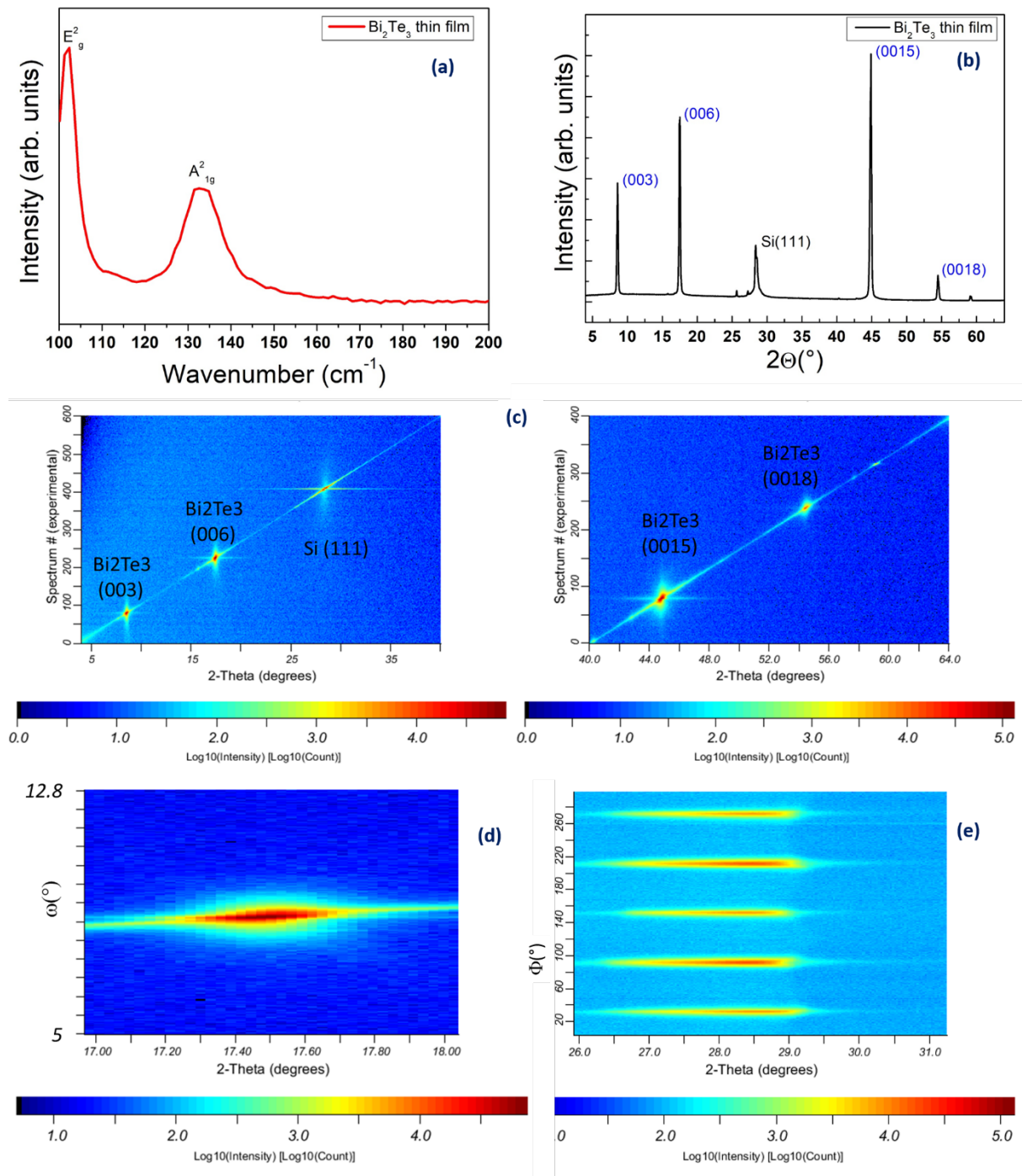
Figure 2. (a) Raman spectrum of Bi_2Te_3 layer, (b) Bragg-Brentano pattern, (c) and (d) Bragg-Brentano maps, (e) phi-scan around the [015] direction of the [001] out-of-plane oriented crystallites.

The Bi_2Te_3 layers were measured by XRD in Bragg Brentano configuration. In Figure 2(b) and 2(c), the XRD pattern exhibited intense reflections at 2θ = 8.46°, 17.3°, 44.8°, and 54.4° corresponding to the 003, 006, and 0015 and 0018 reflections, attributed to the rhombohedral crystalline structure of Bi_2Te_3 in the R$\overline{3}$m space group, (ICSD 74348). The XRD measurements confirmed that the obtained Bi_2Te_3 layers are relaxed, single crystalline, with the *c* lattice parameter equal to 30.4±0.1 Å and [001] out-of-plane oriented on the i- Si (111) substrate.

The XRD patterns collected in the Bragg-Brentano geometry (Figure 2(c)) revealed the scattering of the reflections' intensity across ω. The full width at half maximum (FWHM) of the ω scan, collected for the [006] reflection (see Figure 2d and Supporting Information, Figure S7) showed a very small value of 0.26°, indicating a mosaicity as low as the one that has been obtained by the MOCVD of Bi_2Te_3 on GaAs [42], confirming the excellent quality of the layer. The in-plane orientation of the [00l] out of plane-oriented crystallites was investigated by complete Φ scans around the [015] asymmetric reflection of the Bi_2Te_3 structure. The Φ scan is shown in Figure 2(e). Only six spots were observed, confirming the in-plane alignment of the crystallites, with a six-fold geometry.

High-Resolution TEM (HRTEM) analysis was performed to investigate the material properties at the sub-nanometric scale. A representative cross-sectional HRTEM image of the Bi_2Te_3 thin layer is reported in Figure 3(a). The overview image reveals the high morphological and crystalline quality of the layer with the typical van der Waals gaps separating the QLs along the [00l] direction [27]. The Fast Fourier Transform of the image, taken on the Bi_2Te_3 region only, shown as inset, also highlights the single-crystal nature of the layer and the high degree of order along the c axis. Figure 3(b) reports the high magnification of the interface in the boxed region in Figure 3(a), while Figure 3(c) shows the superposition of the FFTs of Bi_2Te_3 and Si across the interface. The relative orientations of the FFT patterns demonstrate the epitaxial relationship Bi_2Te_3 [001]‖Si[111] between the layer and the substrate. The out-of-plane and in-plane lattice constants of the Bi_2Te_3 layer, calculated from the FFT, were found to be *c* = 30.5 Å and *a* = 4.4 Å, respectively, in accordance with the bulk lattice parameters of Bi_2Te_3 (ICSD 74348) and the values calculated by the XRD analysis. The same value of the unit cell along the [001] axis was found by measuring the distance between the van der Waals gaps in high-

resolution HAADF (Supporting Information, Figure S8). The QL spacing indicated for Bi_2Te_3 is 1.00 nm. The large overview image reveals the high crystalline quality of the thin layer.
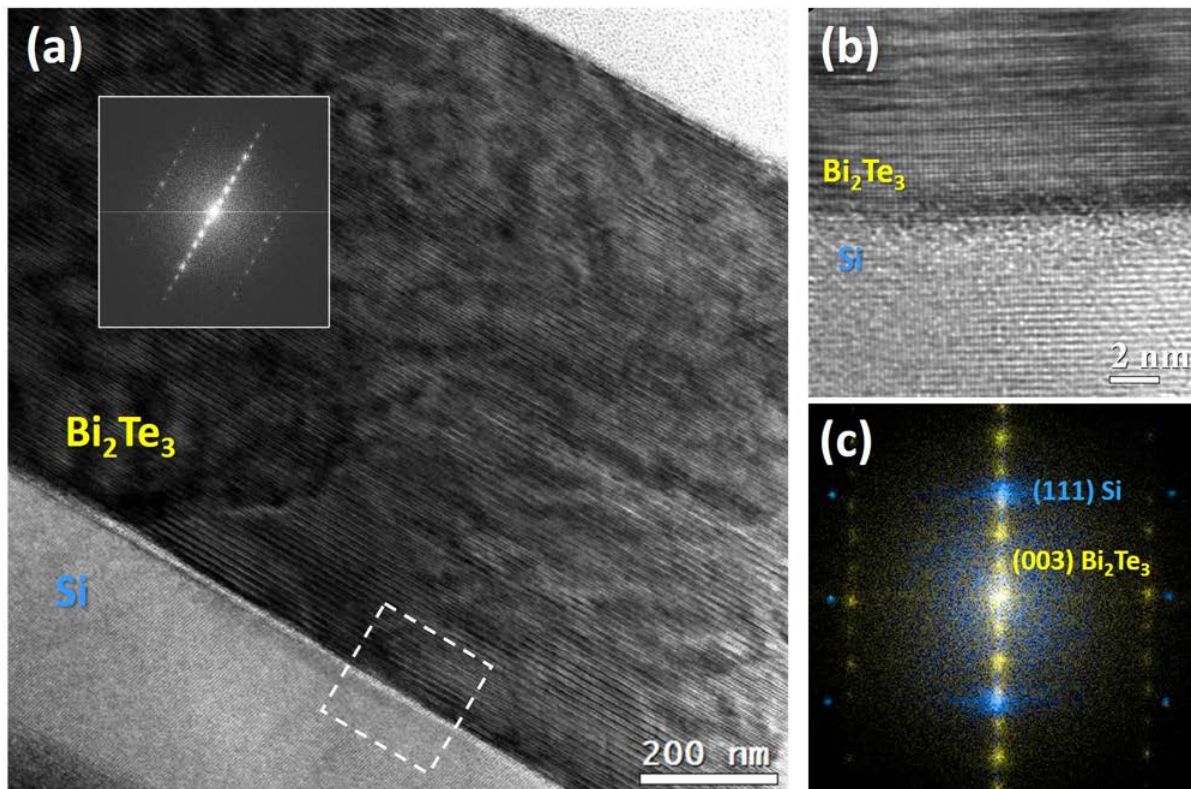

Figure 3. (a) HRTEM image of a Bi_2Te_3 layer on Si substrate with the corresponding FFT in the inset; (b) magnified HRTEM image of the interface in the boxed region in (a); (c) superposition of the FFT patterns of [-1-20] zone axis of Bi_2Te_3 (yellow) and [11-2] zone axis of Si (blue).

The layers were found to be stoichiometric also at the local scale by performing TEM-EDX measurements (see Supporting Information Figure S9 and Table S1). In Figure S8, a typical image of a sample cross-section, taken in the HAADF (Z contrast) mode, is shown. The picture in Figure S9(a) shows a very good thickness uniformity, observed all over the investigated sample. Figure S9(b) and S9 (c), represent the elemental mapping of Te and Bi, obtained with their X-ray L lines, respectively. The two elements appeared to be homogeneously distributed and the stoichiometry preserved everywhere in the sample.

In the literature, both theoretical and experimental results have demonstrated that stoichiometric Bi_2Te_3 is also a TI with time-reversal-symmetry protected surface states that are present in its bulk insulating gap [3,43,44]. Figure 4 shows the comparison between the magneto conductance ($\Delta\sigma$) obtained when the field is applied perpendicularly to the plane of the sample ($\theta = 90°$) and parallelly to it ($\theta = 0°$). The $\theta = 90°$ condition shows a cusp-like shape close to 0 T that overlaps with the ordinary Lorentzian B^2 term. The comparison between

the $\theta = 90°$ and $0°$ conditions points to an interpretation in terms of a 2D-type of conduction mechanism emerging at low temperature [45,46]. In fact, as clearly shown in the inset of Figure 4, by following the subtraction of the Lorentzian B^2 term from the MC at $\theta = 90°$, the typical cusp due to WAL [47] is now clear-cut. This shape of the $\Delta\sigma$ is accepted as a marker of a 2D-type of conduction promoted by the contribution of topological surface states to the transport mechanism [48]. Upon comparing with the published literature [46], we observed that the amplitude of the $\Delta\sigma$ presented for perpendicular field is similar to ours results at the same applied field, expressed in unit of e^2/h.
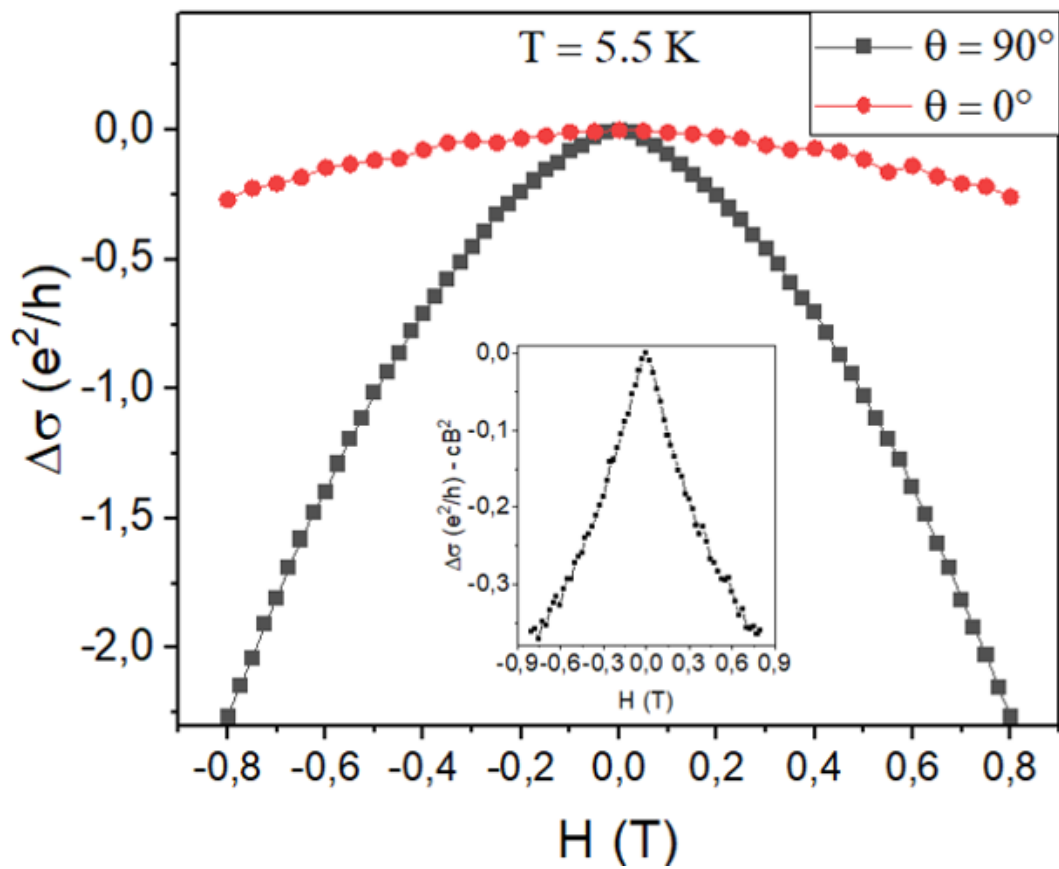

Figure 4: Magneto conductance referred to its zero field value and expressed in unit of e^2/h. The data are collected at 5.5 K on a square macroscopic sample of Bi_2Te_3.

Conclusion

We obtained a large area epitaxy of Bi_2Te_3 thin layers directly on i-Si (111) substrates by an MOVPE process and reported the control and optimization of growth conditions, followed by the assessment of the high crystal quality, flat morphology, composition uniformity, as well as the topological insulator character of the electrical transport. The developed MOVPE process provides a route to enable the large-area Bi_2Te_3 technology-transfer and to exploit its topological conduction behaviour in future spintronic devices.

Notes The authors declare no conflict of interest.

References

1. Venkatasubramanian, R.; Colpitts, T.; Watko, E.; Lamvik, M.; El-Masry, N. MOCVD of Bi2Te3, Sb2Te3 and their superlattice structures for thin-film thermoelectric applications. *J. Cryst. Growth* **1997**, *170*, 817–821.

2. Zhang, H.; Liu, C.-X.; Qi, X.-L.; Dai, X.; Fang, Z.; Zhang, S.-C. Topological insulators in Bi2Se3, Bi2Te3 and Sb2Te3 with a single Dirac cone on the surface. *Nat. Phys.* **2009**, *5*, 438–442.

3. Chen, Y.L.; Analytis, J.G.; Chu, J.H.; Liu, Z.K.; Mo, S.K.; Qi, X.L.; Zhang, H.J.; Lu, P.H.; Dai, X.; Fang, Z.; et al. Experimental realization of a three-dimensional topological insulator, Bi2Te3. *Science (80-.).* **2009**, *325*, 178–181, doi:10.1126/science.1173034.

4. Wu, Z.; Mu, E.; Wang, Z.; Chen, X.; Wu, Z.; Liu, Y.; Hu, Z. Bi2Te3 Nanoplates' Selective Growth Morphology on Different Interfaces for Enhancing Thermoelectric Properties. *Cryst. Growth Des.* **2019**, *19*, 3639–3646.

5. Ando, Y. Topological insulator materials. *J. Phys. Soc. Japan* **2013**, *82*, 102001.

6. Dresselhaus, M.S.; Chen, G.; Tang, M.Y.; Yang, R.G.; Lee, H.; Wang, D.Z.; Ren, Z.F.; Fleurial, J.; Gogna, P. New directions for low-dimensional thermoelectric materials. *Adv. Mater* **2007**, *19*, 1043–1053.

7. Nguyen, T.T.T.; Dang, L.T.; Bach, G.H.; Dang, T.H.; Nguyen, K.T.; Pham, H.T.; Nguyen-Tran, T.; Nguyen, T.V.; Nguyen, T.T.; Nguyen, H.Q. Enhanced thermoelectricity at the ultra-thin film limit. *Appl. Phys. Lett.* **2020**, *117*, 083104, doi:10.1063/5.0010274.

8. Hoefer, K.; Becker, C.; Rata, D.; Swanson, J.; Thalmeier, P.; Tjeng, L.H. Intrinsic conduction through topological surface states of insulating Bi2Te3 epitaxial thin films. *Proc. Natl. Acad. Sci. U. S. A.* **2014**, *111*, 14979–14984, doi:10.1073/pnas.1410591111.

9. Qu, D.X.; Hor, Y.S.; Xiong, J.; Cava, R.J.; Ong, N.P. Quantum oscillations and hall anomaly of surface states in the topological insulator Bi2Te3. *Science (80-.).* **2010**, *329*, 821–824, doi:10.1126/science.1189792.

10. Alpichshev, Z.; Analytis, J.G.; Chu, J.-H.; Fisher, I.R.; Chen, Y.L.; Shen, Z.-X.; Fang, A.; Kapitulnik STM imaging of electronic waves on the surface of Bi2Te3: topologically protected surface states and hexagonal warping effects. *Phys. Rev. Lett.* **2010**, *104*, 16401.

11. Vobornik, I.; Manju, U.; Fujii, J.; Borgatti, F.; Torelli, P.; Krizmancic, D.; Hor, Y.S.; Cava, R.J.; Panaccione, G. Magnetic proximity effect as a pathway to spintronic applications of

topological insulators. *Nano Lett.* **2011**, *11*, 4079–4082.

12. Gupta, B.K.; Sultana, R.; Singh, S.; Singh, V.; Awana, G.; Gupta, A.; Singh, B.; Srivastava, A.K.; Srivastava, O.N.; Auluck, S.; et al. Unexplored photoluminescence from bulk and mechanically exfoliated few layers of Bi2Te3. *Sci. Rep.* **2018**, *8*, 1–6.

13. Lee, H.-Y.; Chen, Y.-S.; Lin, Y.-C.; Wu, J.-K.; Lee, Y.-C.; Wu, B.-K.; Chern, M.-Y.; Liang, C.-T.; Chang, Y.H. Epitaxial growth of Bi2Te3 topological insulator thin films by temperature-gradient induced physical vapor deposition (PVD). *J. Alloys Compd.* **2016**, *686*, 989–997.

14. Concepción, O.; Pereira, V.M.; Choa, A.; Altendorf, S.G.; Escobosa, A.; de Melo, O. The growth of Bi2Te3 topological insulator films: Physical vapor transport vs molecular beam epitaxy. *Mater. Sci. Semicond. Process.* **2019**, *101*, 61–66.

15. Qiao, J.; Zhao, Y.; Jin, Q.; Tan, J.; Kang, S.; Qiu, J.; Tai, K. Tailoring nanoporous structures in Bi2Te3 thin films for improved thermoelectric performance. *ACS Appl. Mater. Interfaces* **2019**, *11*, 38075–38083.

16. Kurokawa, T.; Mori, R.; Norimasa, O.; Chiba, T.; Eguchi, R.; Takashiri, M. Influences of substrate types and heat treatment conditions on structural and thermoelectric properties of nanocrystalline Bi2Te3 thin films formed by DC magnetron sputtering. *Vaccum* **2020**, 109535.

17. Sudarshan, C.; Jayakumar, S.; Vaideki, K.; Nandy, S.; Sudakar, C. Structural, electrical, optical and thermoelectric properties of e-beam evaporated Bi-rich Bi2Te3 thin films. *Thin Solid Films* **2019**, *672*, 165–175.

18. Das, J.K.; Nahid, M.A.I. Electrical Properties of Thermal Evaporated Bismuth Telluride Thin Films. *Int. J. Thin Film. Sci. Technol.* **2015**, *4*, 13.

19. Dauscher, A.; Thomy, A.; Scherrer, H. Pulsed laser deposition of Bi2Te3 thin films. *Thin Solid Films* **1996**, *280*, 61–66.

20. Liao, Z.; Brahlek, M.; Ok, J.M.; Nuckols, L.; Sharma, Y.; Lu, Q.; Zhang, Y.; Lee, H.N. Pulsed-laser epitaxy of topological insulator Bi2Te3 thin films. *A P L Mater.* **2019**, *7*, 41101.

21. Díaz, O.C.; de Melo Pereira, O.; Echavarría, A.E. Substrate influence on preferential orientation of Bi2Te3 layers grown by physical vapor transport using elemental Bi and Te sources. *Mater. Chem. Phys.* **2017**, *198*, 341–345.

22. Concepcion, O.; Galvan-Arellano, M.; Torres-Costa, V.; Climent-Font, A.; Bahena, D.; Manso Silvan, M.; Escobosa, A.; de Melo, O. Controlling the epitaxial growth of Bi2Te3, BiTe, and

Bi4Te3 pure phases by physical vapor transport. *Inorg. Chem.* **2018**, *57*, 10090–10099.

23. Concepción, O.; Tavira, A.; Roque, J.; de Melo, O.; Escobosa, A. Texture analysis and epitaxial relationships in Bi2Te3 thin film grown by physical vapor transport on silicon substrates. *Appl. Surf. Sci.* **2019**, *464*, 280–286.

24. Thorat, J.B.; Mohite, S. V; Madake, S.B.; Suryavanshi, R.D.; Rajpure, K.Y.; Shinde, T.J.; Fulari, V.J.; Shinde, N.S. Electrochemical and surface deformation studies on electrodeposited nanostructured Bi2Te3 thin films. *Opt. Technol. Laser* **2019**, *113*, 384–393.

25. He, L.; Kou, X.; Wang, K.L. Review of 3D topological insulator thin-film growth by molecular beam epitaxy and potential applications. *Phys. status solidi - Rapid Res. Lett.* **2013**, *7*, 50–63.

26. Ginley, T.P.; Wang, Y.; Law, S. Topological insulator film growth by molecular beam epitaxy: A review. *Crystals* **2016**, *6*, 154.

27. Kampmeier, J.; Borisova, S.; Plucinski, L.; Luysberg, M.; Mussler, G.; Grützmacher, D. Suppressing twin domains in molecular beam epitaxy grown Bi2Te3 topological insulator thin films. *Cryst. Growth Des.* **2015**, *15*, 390–394.

28. Harrison, S.E.; Li, S.; Huo, Y.; Zhou, B.; Chen, Y.L.; Harris, J.S. Two-step growth of high quality Bi2Te3 thin films on Al2O3 (0001) by molecular beam epitaxy. *Appl. Phys. Lett.* **2013**, *102*, 171906.

29. Liu, H.W.; Yuan, H.T.; Fukui, N.; Zhang, L.; Jia, J.F.; Iwasa, Y.; Chen, M.W.; Hashizume, T.; Sakurai, T.; Xue, Q.K. Growth of topological insulator Bi2Te3 ultrathin films on Si(111) investigated by low-energy electron microscopy. *Cryst. Growth Des.* **2010**, *10*, 4491–4493, doi:10.1021/cg1007457.

30. Borisova, S.; Krumrain, J.; Luysberg, M.; Mussler, G.; Grützmacher, D. Mode of growth of ultrathin topological insulator Bi2Te 3 films on Si (111) substrates. *Cryst. Growth Des.* **2012**, *12*, 6098–6103, doi:10.1021/cg301236s.

31. Giani, A.; Boulouz, A.; Pascal-Delannoy, F.; Foucaran, A.; Charles, E.; Boyer, A. Growth of Bi2Te3 and Sb2Te3 thin films by MOCVD. *Mater. Sci. Eng. B* **1999**, *64*, 19–24.

32. Kang, S.; Jeon, K.; Shin, J.; Chun, J.; Kim, Y.; Lee, S.J.; Yun, J. MOCVD of C-oriented Bi2Te3 Films on SiO2 Substrates using Triethyl Bismuth and Di-tertiarybutyl Tellurium. *Chem. Vap. Depos.* **2013**, *19*, 61–67.

33. Kuznetsov, P.I.; Yapaskurt, V.O.; Shchamkhalova, B.S.; Shcherbakov, V.D.; Yakushcheva, G.G.;

Luzanov, V.A.; Jitov, V.A. Growth of Bi2Te3 films and other phases of Bi-Te system by MOVPE. *J. Cryst. Growth* **2016**, *455*, 122–128.

34. Jin, H.; Kim, K.-C.; Seo, J.; Kim, S.K.; Cheong, B.; Kim, J.-S.; Lee, S. High mobility, large linear magnetoresistance, and quantum transport phenomena in Bi2Te3 films grown by metallo-organic chemical vapor deposition (MOCVD). *Nanoscale* **2015**, *7*, 17359–17365.

35. Cao, H.; Venkatasubramanian, R.; Liu, C.; Pierce, J.; Yang, H.; Zahid Hasan, M.; Wu, Y.; Chen, Y.P. Topological insulator Bi2Te3 films synthesized by metal organic chemical vapor deposition. *Appl. Phys. Lett.* **2012**, *101*, 162104.

36. Teweldebrhan, D.; Goyal, V.; Balandin, A.A. Exfoliation and characterization of bismuth telluride atomic quintuples and quasi-two-dimensional crystals. *Nano Lett.* **2010**, *10*, 1209–1208, doi:10.1021/nl903590b.

37. Steiner, H.; Volobuev, V.; Caha, O.; Bauer, G.; Springholz, G.; Holý, V. Structure and composition of bismuth telluride topological insulators grown by molecular beam epitaxy. *J. Appl. Crystallogr.* **2014**, *47*, 1889–1900, doi:10.1107/S1600576714020445.

38. Shen, J.; Cha, J.J. Topological crystalline insulator nanostructures. *Nanoscale* 2014, *6*, 14133–14140.

39. Krumrain, J.; Mussler, G.; Borisova, S.; Stoica, T.; Plucinski, L.; Schneider, C.M.; Grützmacher, D. MBE growth optimization of topological insulator Bi2Te3 films. *J. Cryst. Growth* **2011**, *324*, 115–118, doi:10.1016/j.jcrysgro.2011.03.008.

40. Mzerd, A.; Sayah, D.; Brun, G.; Tedenac, J.C.; Boyer, A. Crystal growth and sticking coefficient of Bi2Te3 thin films on Si(1 1 1) substrate. *J. Mater. Sci. Lett.* **1995**, *14*, 194–197, doi:10.1007/BF00318254.

41. Shahil, K.M.F.; Hossain, M.Z.; Goyal, V.; Balandin, A. Micro-Raman spectroscopy of mechanically exfoliated few-quintuple layers of Bi2Te3, Bi2Se3, and Sb2Te3 materials. *J. Appl. Phys.* **2012**, *111*, 54305.

42. Jin, H.; Kim, K.C.; Seo, J.; Kim, S.K.; Cheong, B.K.; Kim, J.S.; Lee, S. High mobility, large linear magnetoresistance, and quantum transport phenomena in Bi2Te3 films grown by metallo-organic chemical vapor deposition (MOCVD). *Nanoscale* **2015**, *7*, 17359–17365, doi:10.1039/c5nr05491e.

43. Zhang, H.; Liu, C.-X.; Qi, X.-L.; Dai, X.; Fang, Z.; Zhang, S.-C. Topological Insulators in Bi2Se3, Bi2Te3 and Sb2Te3 with single Dirac cone on the surface. *Nat. Phys.* **2009**, *5*, 438–442.

44. Li, Y.Y.; Wang, G.; Zhu, X.G.; Liu, M.H.; Ye, C.; Chen, X.; Wang, Y.Y.; He, K.; Wang, L.L.; Ma, X.C.; et al. Intrinsic topological insulator Bi2Te3 thin films on si and their thickness limit. *Adv. Mater.* **2010**, *22*, 4002–4007, doi:10.1002/adma.201000368.

45. Roy, A.; Guchhait, S.; Sonde, S.; Dey, R.; Pramanik, T.; Rai, A.; Movva, H.C.P.; Colombo, L.; Banerjee, S.K. Two-dimensional weak anti-localization in Bi2Te3 thin film grown on Si(111)-(7 × 7) surface by molecular beam epitaxy. *Appl. Phys. Lett.* **2013**, *102*, 163118, doi:10.1063/1.4803018.

46. Zhang, S.X.; Yan, L.; Qi, J.; Zhuo, M.; Wang, Y.Q.; Prasankumar, R.P.; Jia, Q.X.; Picraux, S.T. Epitaxial thin films of topological insulator Bi2Te3 with two-dimensional weak anti-localization effect grown by pulsed laser deposition. *Thin Solid Films* **2012**, *520*, 6459–6462, doi:10.1016/j.tsf.2012.07.012.

47. Hikami, S.; Larkin, A.I.; Nagaoka, Y. Spin-Orbit Interaction and Magnetoresistance in the Two Dimensional Random System. *Prog. Theor. Phys.* **1980**, *63*, 707–710, doi:10.1143/ptp.63.707.

48. Shrestha, K.; Chou, M.; Graf, D.; Yang, H.D.; Lorenz, B.; Chu, C.W. Extremely large nonsaturating magnetoresistance and ultrahigh mobility due to topological surface states in the metallic Bi2Te3 topological insulator. *Phys. Rev. B* **2017**, *95*, 195113, doi:10.1103/PhysRevB.95.195113.